Macrophage Cholesterol Homeostasis Underpins the role of Sertraline as an Adjunctive Agent in Tuberculosis Therapy.

Kanika Bisht [1,2], Riya Sahu [1,2], Sneha Vasudevan [3], Simran Jit [1,2], Nikita Bhor [1,2], Jitendra Kumar [1], Mahima Madan [1,2], Deepthi Shankaran [1,2], Sherry Bhalla [1,2], Nagasuma Chandra [3], Vivek Rao [1,2]*

1-CSIR- Institute of Genomics and Integrative Biology, Mathura Road, New Delhi-110025 India.

2- Academy of Scientific and Innovative Research (AcSIR), Ghaziabad, 201002, India

3-IISc Mathematics Initiative, Indian Institute of Science, Bangalore 560012, India, Department of Biochemistry, Indian Institute of Science, Bangalore 560012, India, Centre for Biosystems Science and Engineering, Indian Institute of Science, Bangalore 560012, India

*Corresponding author: Tel: +91 11 29879229, E-mail: vivek.rao@igib.res.in.

Key words: *Mycobacterium tuberculosis*/ host-directed therapy/ antidepressant/ sertraline

Running Title: Cholesterol flux dictates bacterial control

Abstract:

An intricate relationship exists between metabolism and the macrophage response in controlling intracellular pathogens such as Mycobacterium tuberculosis (Mtb). Here, we identify a deterministic role for macrophage cholesterol metabolism in the efficacy of anti-tubercular therapy (ATT). We found that sertraline (SRT), an FDA-approved antidepressant capable of enhancing tuberculosis treatment, rewires the macrophage lipid metabolism to potentiate Mtb clearance. Treatment with SRT leads to lysosomal cholesterol accumulation, thereby activating the cholesterol-sensing transcription factor SREBP2 and increasing biosynthetic cholesterol flux in macrophages. In addition, this buildup of cholesterol induces lysosomal membrane permeabilization (LMP), mitochondrial ROS production, and downstream NLRP3 inflammasome activation, contributing to enhanced macrophage-mediated bacterial killing. Our results thus highlight a previously underappreciated link between cholesterol homeostasis and inflammasome

activation, which contributes to improved Mtb clearance in the presence of adjunctive sertraline therapy.

Graphical abstract:

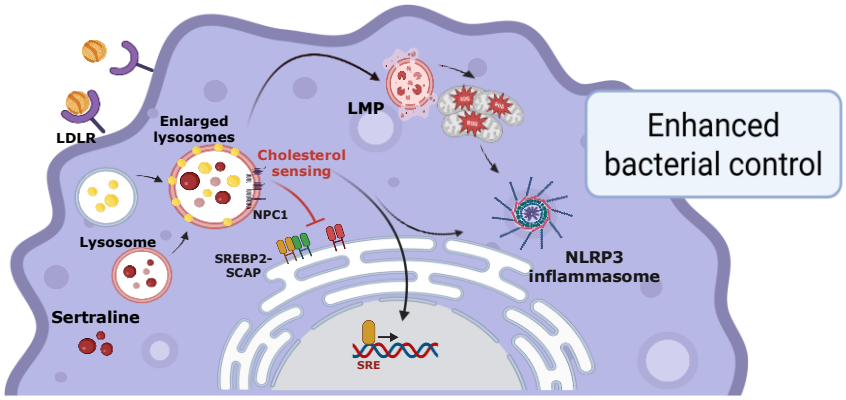

SRT induced lysosomal cholesterol accumulation results in enhanced bacterial control via inflammasome activation

Introduction:

Tuberculosis (TB), caused by *Mycobacterium tuberculosis* (Mtb), remains the leading cause of death by a single infectious agent globally, outpacing all other bacterial and viral pathogens [1-3]. The multiple initiatives to curb the infection have not been successful enough to eradicate the disease, instead have led to an increase in drug resistance in the population [4,5]. These limitations have spurred an interest in therapeutic strategies designed to aid the host in controlling infection. Such host-directed therapies (HDTs) have relied on harnessing the cellular physiological pathways to enhance antimicrobial properties [6-8]. We have previously shown that sertraline (SRT), a selective serotonin reuptake inhibitor (SSRI), can act as a potent adjunct to standard anti-TB therapy (ATT), accelerating bacterial clearance, improving tissue resolution, and enhancing host survival in preclinical infection models [9]. These properties are associated with the restriction of type I IFN responses via the activation of the host inflammasome pathway, thus defining the therapeutic potential of manipulating host immunity for infection control [10].

Recent findings strongly advocate for the influence of host sterol metabolism in regulating the inflammatory capacity of innate immune cells [11-13]. More importantly, oxysterols have emerged as promoters of the pro-inflammatory capacity of macrophages [14,15]. Recently, SREBP2, the master

53 regulator of cellular cholesterol metabolism has been associated with the directly activation of the
54 host cell inflammasomes via the NLRP3 axis [16].
55 Here, we demonstrate that treatment with SRT leads to a significant increase in intracellular
56 cholesterol levels in Mtb-infected macrophages—an effect critical for enhanced bacterial control.
57 In light of these observations, we sought to investigate whether the adjunctive efficacy of sertraline
58 is mechanistically linked to its influence on host cholesterol metabolism. By employing chemical
59 modulation and gene silencing, we demonstrate that the SRT-mediated cholesterol buildup
60 perturbs lysosomal integrity, thereby promoting mitochondrial reactive oxygen species (ROS)
61 production and thus cascading into the activation of the NLRP3 inflammasome. Taken together,
62 our findings provide a mechanistic link between cellular metabolic machinery, particularly
63 cholesterol metabolism, and antimicrobial efficacy, offering both conceptual and translational
64 insights into how metabolic reprogramming can be leveraged for augmenting host immunity as a
65 host-directed therapeutic strategy to improve TB treatment outcomes.

66 **Results:**

67 **Treatment with sertraline increases cellular cholesterol in macrophages**

68 In an attempt to decipher the underlying mechanism for sertraline- mediated increase of antibiotic
69 efficacy in Mtb infections, global expression profiles of Mtb-infected THP1 macrophages with a
70 combination of isoniazid (H) and rifampicin (R) with (SRT) were compared with HR-treated cells.
71 A total of 160 genes of cholesterol homeostasis were differentially upregulated on treatment with
72 HRS when compared to HR treatment (Figure 1A). Interestingly, cholesterol homeostasis
73 emerged as the most significantly enhanced metabolic pathway along with an increase in the
74 mTORC1 signaling complex in macrophages treated with HRS (Figure 1B). In fact, HRS-treated
75 macrophages displayed a significant increase in the expression of genes involved in cholesterol
76 biosynthesis (Figure 1C) and import, with the markedly lower expression of sterol export genes
77 (Figure 1D). A similar pattern was reflected in SRT or HRS-treated macrophages by qRT-PCR.
78 While infection or treatment with HR failed to alter the expression of genes involved in cholesterol

79 metabolism, genes involved in biosynthesis and import were 3-5-fold higher with treatment with
80 HRS or SRT at 24 h of infection (Figure 1E). This increment in gene expression reflected as an
81 SRT-dependent 1.2-1.5-fold increase in intracellular cholesterol (Figure 1F). To specifically inhibit
82 cholesterol biosynthesis, we employed a pharmacological inhibitor of *HMGCR*, simvastatin.
83 Contrary to our expectations of diminishing antibiotic efficacy, the addition of simvastatin
84 significantly enhanced the control of Mtb by antibiotics by 3-5-fold in comparison to the cells
85 treated with HR or HRS alone (Figure 1G). Previous reports have suggested that statins, in turn,
86 can enhance expression of genes in cholesterol biosynthesis [17], we also tested for the gene
87 expression following treatment with statins. Treatment with simvastatin induced the expression of
88 the genes of the biosynthetic pathway as well as genes of cholesterol import. Also, a decrease in
89 the cholesterol export genes has been observed with simvastatin treatment (Figure 1H). This
90 suggested that the increased flux of the pathway may be crucial in enhancing bacterial control by
91 SRT.
92
93
94
95
96
97
98
99
100
101
102
103
104

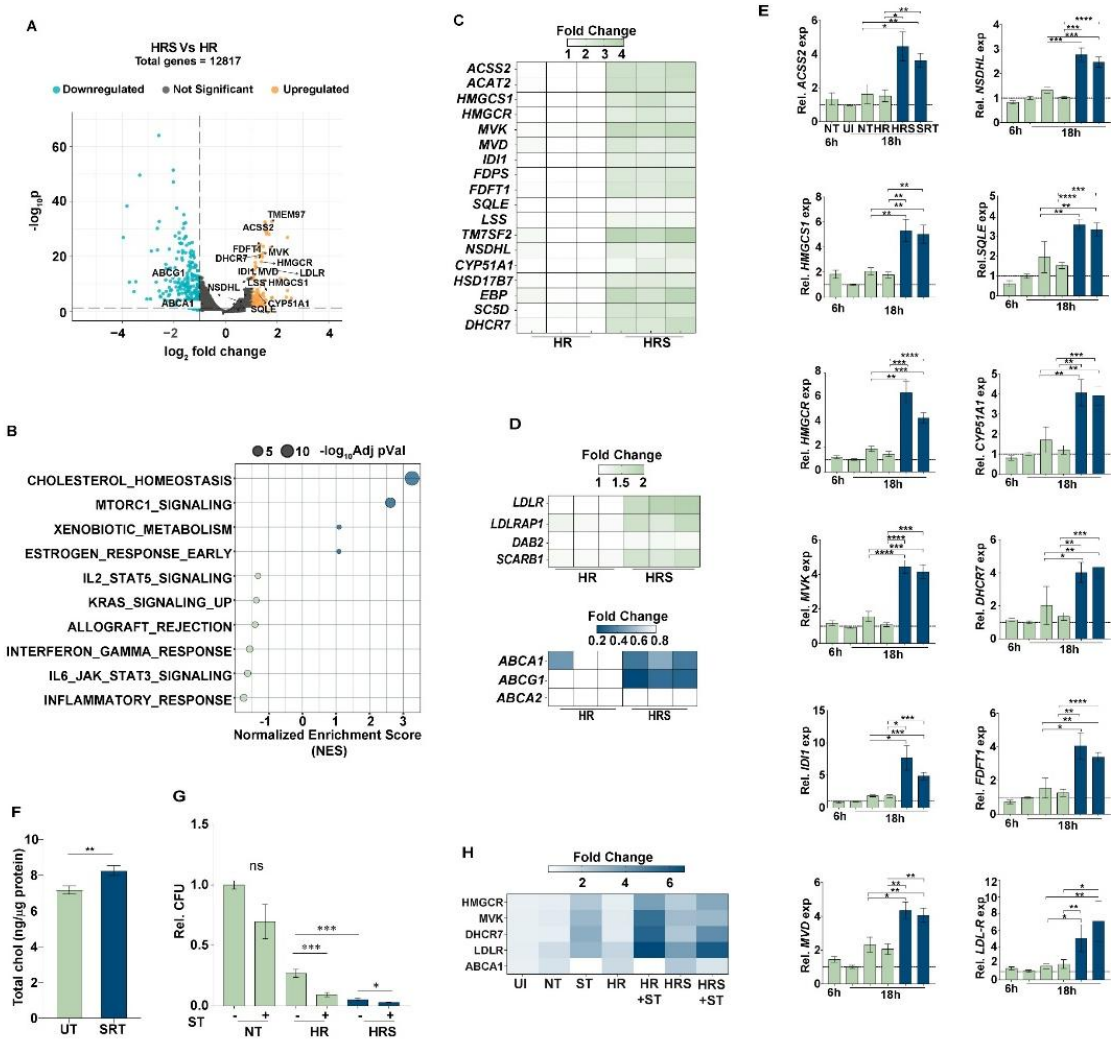

Figure 1

Figure 1: Global transcriptomics of Mtb-infected macrophages following treatment with sertraline.

A) A comparison of the differentially expressed genes in Mtb-infected macrophages following an 18 h treatment with HR or HRS is shown as a volcano plot. Y- and X-axes denote the $-\log_{10}$ P values and $\log_2$ fold change, respectively. The upregulated genes with ≥ 2 fold change with p-value of ≤ 0.01 are highlighted in orange, while the downregulated genes with ≤ -2 fold change with p-value of ≤ 0.01 are in blue.

B) GSEA analysis of the top significantly enriched gene sets in HRS vs HR is represented as a bubble plot. Gene sets that are significantly (P-value ≤ 0.05, 0.01) enriched (Blue) or

131 downregulated (green) are represented, with the X-axis denoting the normalized
132 enrichment score.
133 C-E) Gene expression patterns in HR and HRS-treated macrophages: Expression of genes
134 involved in cholesterol biosynthesis (C) and cholesterol trafficking (D) in the RNA-seq data
135 was validated by gene-specific qRT-PCR (E). The relative expression of specific genes
136 relative to *GAPDH* is represented as fold change w.r.t uninfected control (UI) at 6h ± SEM
137 of triplicate assays from 3 independent experiments (N=3).
138 F) Cholesterol levels in THP1 macrophages after treatment with sertraline (SRT) for 24 hours.
139 Total free cholesterol was normalized to the amount of protein and is represented as mean
140 ± SEM for triplicate assays of three independent experiments (N=3).
141 G) Growth of Mtb in HR or HRS treated macrophages that were treated with 10μM simvastatin
142 (ST) for 3 days. Bacterial numbers are represented as mean $\log_{10}$ CFU ± SEM from
143 triplicate assays of three or four independent experiments (N = 3 or 4).
144 H) Effect of simvastatin on the expression of genes for biosynthesis (HMGCR, MVK, DHCR7),
145 import (LDLR), and export (ABCA1) of cholesterol in Mtb-infected macrophages, after 18
146 h of treatment. The relative expression of specific genes, normalized to GAPDH, is
147 represented as the fold change ± SEM of triplicate assays from three independent
148 experiments (N = 3).
149 P values less than 0.05, 0.01, 0.005 are represented as *, ** and *** respectively.
150 **Lysosomal cholesterol accumulation is crucial for Mtb control in macrophages**
151 Cholesterol levels in different subcellular locations are tightly regulated to maintain a steady state
152 in cells. To test the effect of increased cellular cholesterol on intracellular distribution,
153 macrophages were stained with the cholesterol specific dye- filipin and visualized by fluorescence
154 microscopy. While filipin staining was primarily concentrated on the membranes of untreated (UT)
155 cells with minimal staining within, treatment with SRT severely impacted intracellular sterol levels,

156 with cells displaying significantly higher intracellular staining in addition to the membrane (Figure
157 2A).
158 To further identify the intracellular niche of the accumulated cholesterol, cells fed with NBD-
159 cholesterol were stained with the lysosomal stain-lysotracker. Again, while in the untreated cells,
160 minimal levels of cholesterol co-localized with lysosomes, the majority of the internalized
161 cholesterol in SRT-treated cells was found to be accumulated in the lysosomal compartments,
162 indicating a pronounced accumulation of cholesterol in the lysosomal compartments with SRT
163 treatment (Figure 2B, C).
164 In order to understand if this increase in cholesterol biosynthesis was a generic property of SSRIs,
165 another widely used antidepressant, citalopram, was tested for its ability to control intracellular
166 bacterial growth. Surprisingly, the addition of citalopram to the frontline TB drugs-HR did not affect
167 bacterial control in macrophages, unlike the increased control of infection by HRS in comparison
168 to the antibiotics alone (Figure 2D). Remarkably, unlike SRT, citalopram failed to induce
169 cholesterol accumulation in the lysosomes or enhance the expression of cholesterol biosynthesis
170 in macrophages, validating the importance of this mechanism in enhanced antibiotic control of
171 Mtb (Figure 2E, F).
172
173

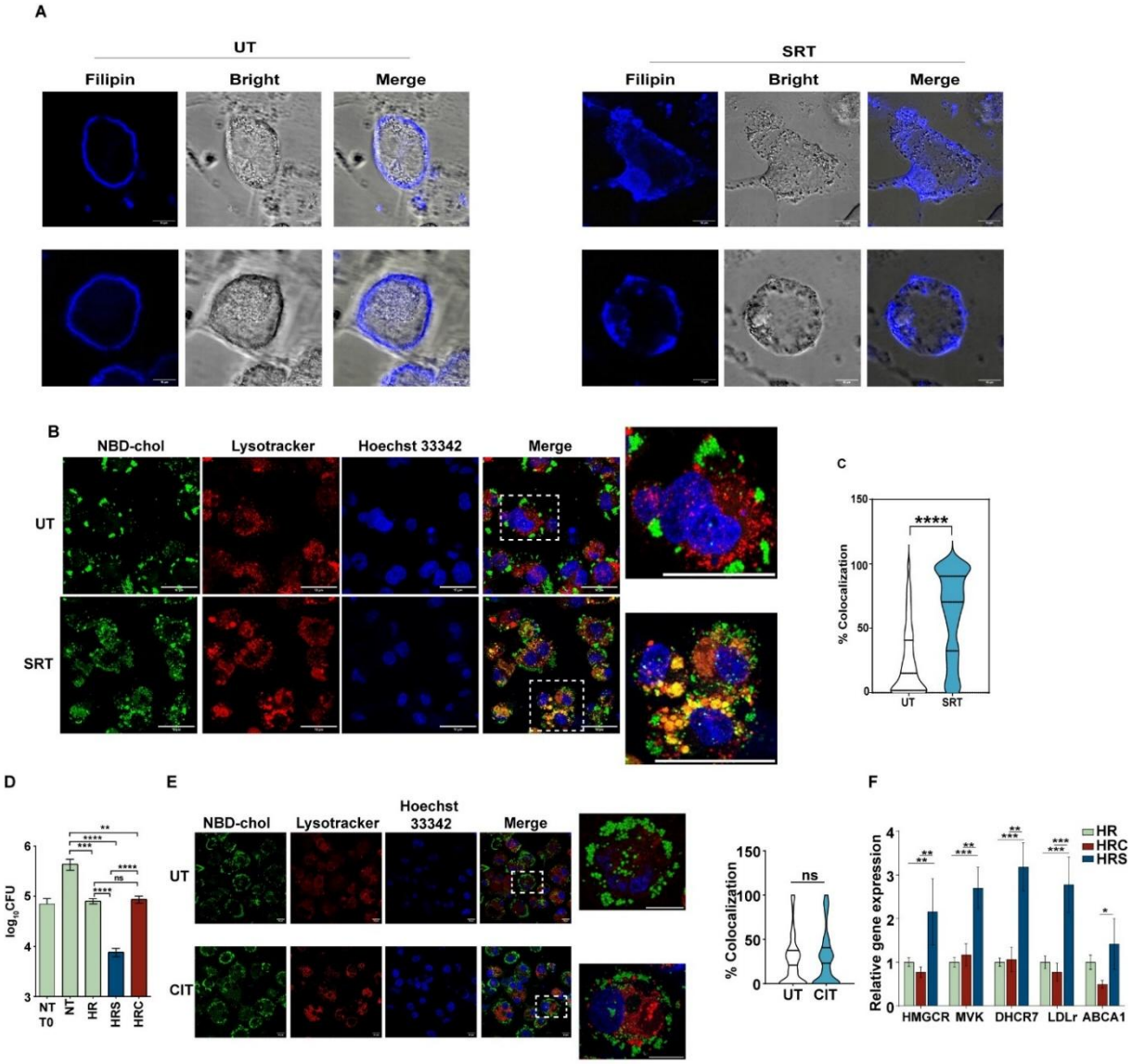

Figure 2

Figure 2: Sertraline treated macrophages accumulate lysosomal cholesterol.

A-B) Representative confocal images of THP1 macrophages after SRT treatment for 24 h, stained with filipin (A) or fed with NBD-cholesterol and stained with lysotracker Red and Hoechst 33342 (B). The inset shows the zoom-in along the black lines. Scale bar = 10μm.

(C) The graph shows the percent colocalization of the NBD-cholesterol in the lysosomes from three independent experiments.

199 D) Intracellular bacterial growth was estimated in Mtb–infected THP1 macrophages left untreated
200 (NT) or treated with HR alone or in combination with 20 μM citalopram (CIT) for 3 days. The data
201 are represented as mean Log_{10} values ± SEM from triplicate assays of four independent
202 experiments (N = 4).
203 E) Representative confocal images of THP1 macrophages treated with citalopram along with
204 NBD-cholesterol for 24 hours and stained with lysotracker Red, and the colocalization percentage
205 is calculated using ImageJ. Scale bar = 10μm.
206 F) Gene expression levels in macrophages infected with Mtb, followed by treatment with HR alone
207 or with citalopram. The relative expression of the specific gene, relative to GAPDH, is represented
208 as fold change with respect to HR ± SEM of triplicate assays from three independent experiments
209 (N=3).
210 P values less than 0.05, 0.01, 0.005 are represented as *, ** and *** respectively.
211
212 **Sertraline enhances SREBP2 activation in macrophages**:
213 The feedback activation of SREBP2 in response to the absence of cholesterol sensing in the ER
214 on account of lysosomal sequestration is well documented [18,19]. To assess whether SRT activates
215 the signaling cascade, levels of mature SREBP2 (mSREBP2) were measured in macrophages
216 following SRT treatment. Indeed, commensurate with the significant induction of the SREBF2
217 gene in HRS-treated macrophages, in both the global transcriptomic data and with qRT-PCR
218 analysis, macrophages treated with SRT harbored ~2-fold higher levels of the cleaved, active
219 form of SREBP2 (mSREBP2) by 24h compared to the untreated cells (Figure 3A-D). The relatively
220 unchanged levels of mSREBP2 in both untreated and citalopram treated cells, lends further
221 support to the importance of this signaling axis in the antibiotic potentiating effect of SRT (Figure
222 3 E, F).
223
224

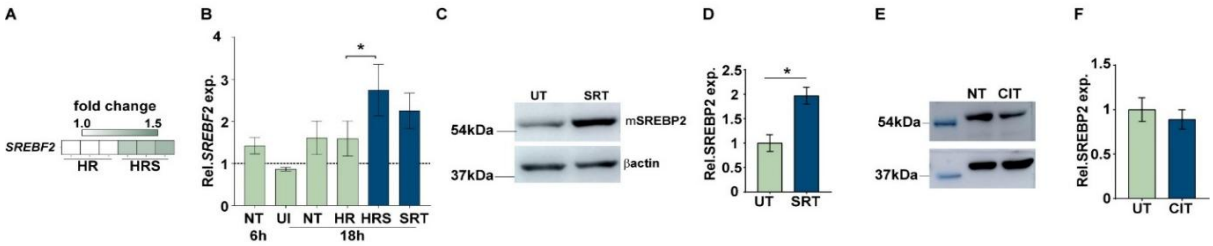

Figure 3: Sertraline enhances SREBP2 activation in macrophages.

A -B) Expression levels of *SREB*F2 in the global transcriptomic analysis dataset (A) or quantified by qRT-PCR (B) in Mtb-infected macrophages left untreated (NT) or treated with HR, HRS, or SRT for 18h. The relative expression of specific genes relative to *GAPDH* is represented as fold change ± SEM of triplicate assays of three independent experiments (N=3).

C-F) The levels of SREBP2 in protein extracts of macrophages left untreated, treated with SRT (C) or 20μM of citalopram (E) for 24 hours were checked by immunoblotting with specific antibodies for SREBP2 and β-actin and quantified by densitometry (D, F). The reactivity for SREBF2 in cells relative to β-actin was quantified in three independent experiments (N=3) and is represented as mean ± SEM.

P values less than 0.05, 0.01 and 0.005 are represented as *, ** and *** respectively.

SREBP2 activation is regulated by multiple feedback mechanisms; typically, cholesterol and oxysterols have been shown to downregulate this process by modulating the SCAP-SREBP2 egress to the Golgi [20]. To test the importance of SREBP2 activation on Mtb control, macrophages were treated with cholesterol exogenously to inhibit SREBP2 processing and tested for their ability to control Mtb growth in the presence of HR or HRS. Addition of cholesterol significantly inhibited SREBP2 activation (2-fold) (Figure 4A, Figure S1A) and resulted in a significant reversal of the effect of SRT on antibiotic potentiation (Figure 4B). Interestingly, even in the HR treated cells, the addition of cholesterol restricted the ability of HR to control bacterial growth with ~2-3-fold higher

251 bacterial numbers (Figure 4B). Further, the inhibition of SREBP2 activation with a specific S2P
252 protease inhibitor- 1,10-phenanthroline, resulted in a significant but partial reversal of bacterial
253 control by SRT (3-4-fold higher bacterial numbers than HRS alone) (Figure 4C). To further test
254 the relevance of SREBP2 processing, macrophages deficient in the SREBP2 cleavage activation
255 protein (SCAP) were tested for their ability to restrict Mtb growth. As expected, THP1 cells with
256 >50% silencing of *SCAP* with specific shRNAs displayed significantly lower levels of SREBP2
257 activation in comparison to the cells treated with scrambled shRNAs (SCR) (Figure 4D-F).
258 Consistent with the inhibition of S2P, silencing of SCAP reduced the effectiveness of SRT on Mtb
259 control without affecting the uptake of bacteria (Figure 4G). As observed in Figure 4G, SCAP-
260 silenced macrophages harbored significantly 3-4 folds higher bacterial numbers than the control
261 cells. Even in the untreated cells, loss of SCAP severely impaired the ability to control Mtb with
262 nearly 3-fold higher CFU in the SCAP-deficient cells than in the control (Inset, Figure 4H),
263 corroborating the requirement of SREBP2 activation in Mtb control by macrophages.

264
265
266
267
268
269
270
271
272
273

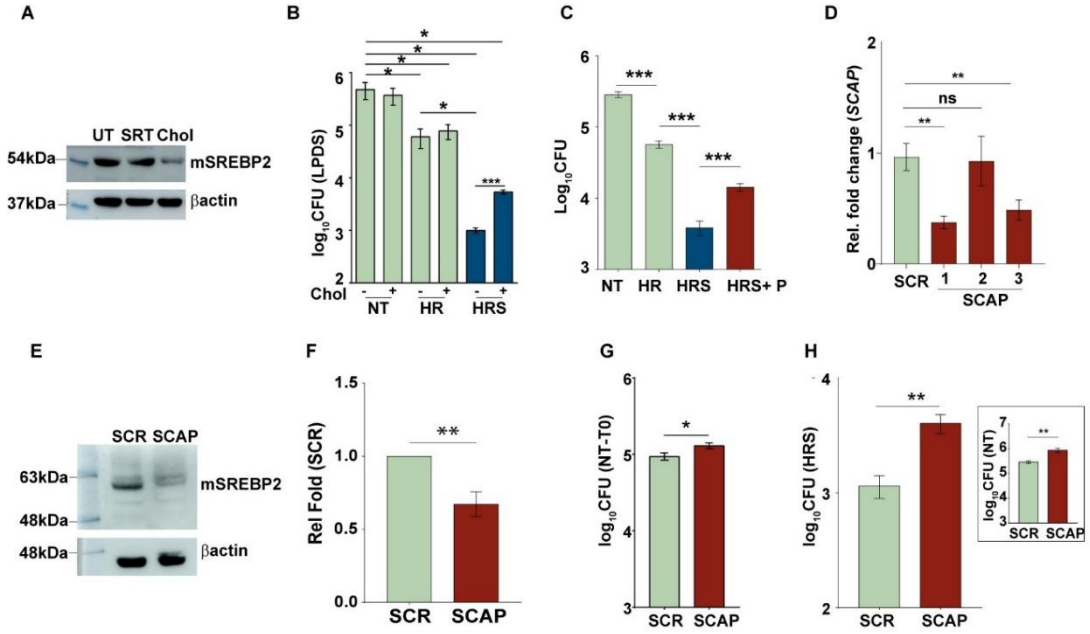

274 Figure 4

275

276 **Figure 4: Role of SREBP2 activation in restricting intracellular bacterial growth.**

277 A) The levels of SREBP2 in cell extracts of macrophages treated with 20µg/ml of cholesterol
278 for 24 h were analysed by immunoblotting. The levels of β-actin were used as the control
279 values for the comparison.
280 B-C) The intracellular bacterial growth was estimated in Mtb-infected macrophages that were
281 either untreated or treated with (B) cholesterol or (C)- 0.5 mM of 1,10-phenanthroline (P)
282 for 1 hour. This was followed by treatment with HR and HRS alone, in combination with
283 cholesterol, which was replenished every 24 hours in the LPDS media, or with 1,10-
284 phenanthroline. The data is represented as mean $\log_{10}$ values ± SEM from triplicate
285 assays of four independent experiments (N = 4).
286 (D) Evaluation of gene expression levels in *SCAP-silenced* macrophages. The relative
287 expression of the *SCAP* is represented as fold change ± SEM w.r.t. scrambled control in
288 triplicate assays from three independent experiments (N=3).
289 (E) Estimation of activation of SREBP2 in protein extracts of *SCAP-silenced* cells by
290 immunoblotting with specific antibodies for SREBP2 and β-actin.
291 (F) Densitometric quantification of the reactivity for SREBP2 in cells relative to β-actin of six
292 independent experiments (N=6) is represented as mean ± SEM.
293 (G) Bacterial uptake in *SCAP-silenced* cells compared to scrambled control after 6 hours of
294 incubation with Mtb at MOI 5.
295 (H) Intracellular growth of Mtb is depicted in untreated (NT) (inset) or HRS-treated *SCAP-*
296 *silenced* cells. The data are represented as mean $\log_{10}$ values ± SEM from triplicate
297 assays of three independent experiments (N = 3).
298
299 **SRT phenocopies the effects of NPC1 inhibition in cells.**
300 A similar phenotype of organellar sterol accumulation, specifically in the endosomal-lysosomal
301 compartments, is a characteristic feature of NPC1 mutation/ deficiency in the human population
302 [21,22]. A strong binding of SRT and the related antidepressant – indatraline, with the N-terminal

303 domain of NPC-1, has been shown to cause accumulation of cholesterol in lysosomes [23]. In order
304 to investigate the relevance of this mechanism, a computational structural analysis using ligand
305 docking for SRT with NPC-1 was performed. The well-established cargo for NPC1- cholesterol,
306 resulted in the identification of a prominent cluster of docked poses with 88% of the docked poses
307 and a mean binding energy of -10.68 kcal/mol (Figure 5A). Having established the correct binding
308 pose, the binding of SRT was tested. Docking of sertraline in the same framework indicated that
309 the docked poses clustered into 2 prominent different clusters, with the top-ranked cluster
310 comprising 56% of the poses, a mean binding energy of -8.28 and -8.13 kcal/mol (Figure 5B).
311 Similar to cholesterol, SRT is also stabilized by hydrophobic interactions and hydrogen bonds,
312 forming a stable protein-ligand complex with a defined pose, indicating its ability to bind to NPC1.
313 Given its inability to impact lysosomal cholesterol distribution, the other SSRI, citalopram, was
314 evaluated for its ability to bind to NPC-1. In contrast to cholesterol and SRT, the docked poses
315 were found to be distributed across six different clusters, with the top-ranked cluster comprising
316 32% of the docked poses (mean binding energy = -7.67 kcal/mol), indicating the absence of a
317 defined pose for citalopram in the NPC1 site, suggestive of poor binding to NPC-1 (Figure 5C).
318 To test the relevance of this binding on bacterial control, the specific inhibitor, U18666A, was
319 tested for its NPC-1 binding capacity and the ability to enhance antibiotic efficacy in macrophages.
320 Surprisingly, U18666A also bound specifically to the same binding pocket as cholesterol with a
321 prominent cluster comprising 92% of the docked poses, having a mean binding energy of -9.66
322 kcal/mol (Figure 5D) (Interactions listed in Suppl table S1). The binding energies computed for
323 the best docked poses of the ligands, cholesterol, and U18666A indicate high affinities in both
324 cases (binding energies -10.82 kcal/mol and -9.71 kcal/mol, respectively), possibly due to the
325 stabilization by a large number of hydrophobic interactions. While the best docked poses of SRT
326 also indicated a high affinity (binding energy –8.31 kcal/mol), citalopram bound NPC1 at a lower
327 affinity of -7.88 kcal/mol (Figure 5E).
328

329 In addition, Citalopram had a higher torsional penalty than SRT, lending it a poorer ligand to NPC1
330 as compared to sertraline (Figure 5F). Further analysis of cholesterol levels in U18666A-treated
331 macrophages revealed a pronounced accumulation in the lysosomal compartments with the
332 consequent SREBP2 activation, with an enhanced expression of the cholesterol biosynthetic
333 machinery similar to SRT (Figure 5G, H, S1B). To verify the importance of increased SREBP2
334 processing in Mtb control, the effect of antibiotics was tested in cells treated with U18666A.
335 Addition of U18666A to the frontline TB drugs -HR resulted in a 3-4-fold better control of Mtb in
336 macrophages by day 3 of infection, emphasizing the relevance of lysosomal cholesterol loading
337 in bacterial control (Figure 5I). To simulate conditions of enhanced cholesterol biosynthesis via
338 increased SREBP2 activation, we resorted to silencing INSIG1, the inhibitor of SCAP-SREBP2
339 translocation for processing and activation at the Golgi, and observed a significant (>60%)
340 decrease in the levels of INSIG1 expression (Figure 5J). However, we did not observe any
341 detectable change in the levels of SREBP2 activation in these macrophages (Figure S1C). As an
342 alternative, macrophages were treated with brefeldin A (BFA) to facilitate constitutive proteolysis
343 and activation of SREBP2 due to the collapse of the ER-Golgi network[24]. In sync with our
344 expectations, the addition of BFA significantly increased the expression of active SREBP2 in
345 macrophages (2-fold- Figure 5K, Figure S1D) that reflected as a 3-4-fold decrease in bacterial
346 numbers in HR treated cells, further emphasizing the importance of SRT-mediated increase in
347 SREBP2 activation in the ability of macrophages to restrict bacteria (Figure 5L).

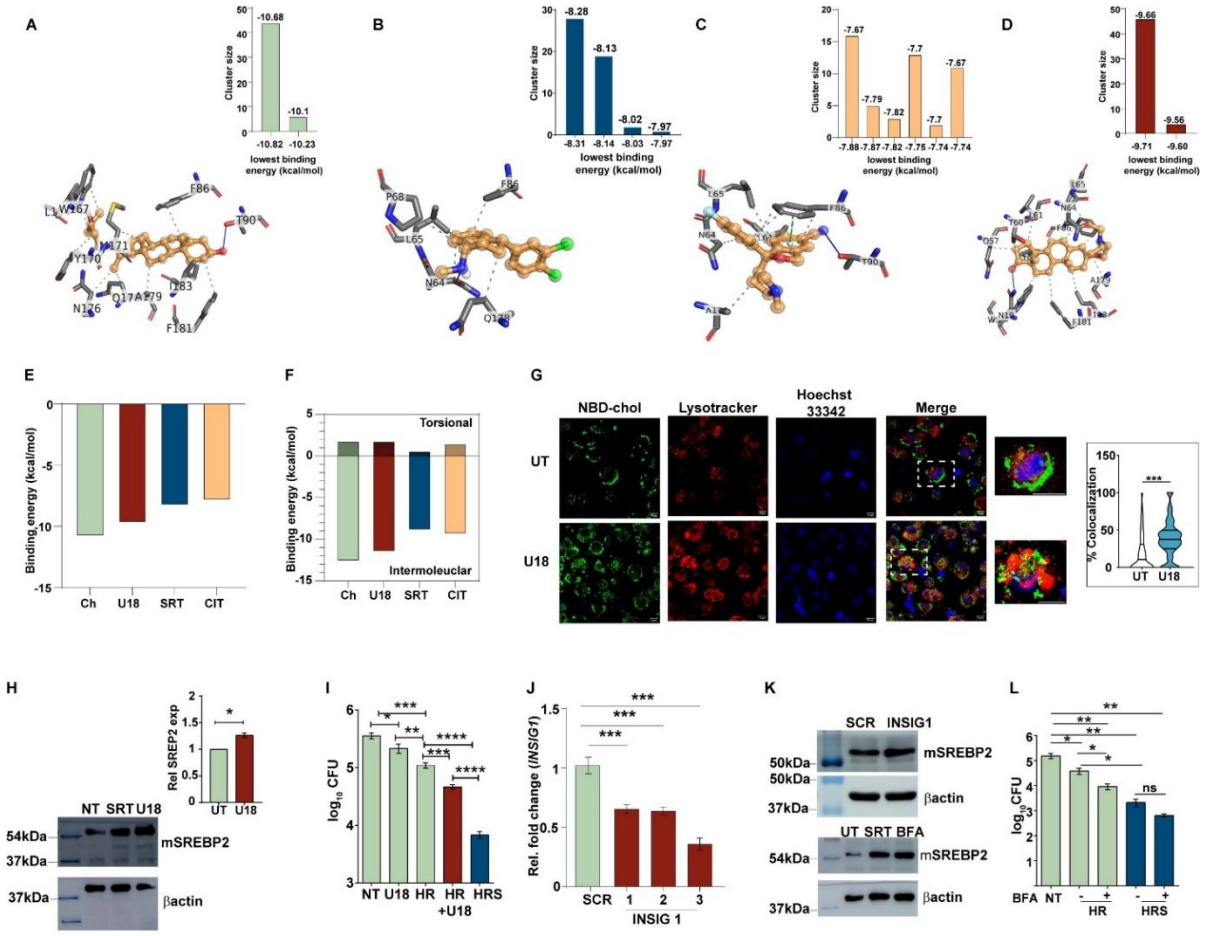

Figure 5

Figure 5: SRT treatment phenocopies NPC1 deficiency.

A-D) The best docked poses for Cholesterol (A), Sertraline (B), Citalopram (C), and U18666A (D), having the lowest binding energy. Bar plots represent the clusters of docked poses and binding sites (Mean binding energy (kcal/mol) for each cluster is mentioned at the top of the bar). Grey dotted line: hydrophobic interactions, blue solid line: hydrogen bonds, green dotted line: pi-pi stacking.

E-F) The bar plots represent the overall binding energy of each ligand (E), and (F) shows the breakdown of the overall binding energy into intermolecular energy and torsional penalty components.

373 G) The localization of cholesterol was analysed in cells treated with 2.5 μg/ml of the NPC1
374 inhibitor- U18666A (U18). The extent of colocalization of NBD-cholesterol and lysosomes
375 (lysotracker) in macrophages was quantified and is expressed as percent co-localization from
376 three independent experiments (N=3) (inset).
377 H) The extent of SREBP2 activation was evaluated in macrophages left untreated or treated with
378 U18666A by immunoblotting and densitometric analysis of the lysates. Levels of β-actin
379 expression were used as the control. The relative levels of mSREBP2 in SRT-treated cells (w.r.t.
380 untreated) are represented as relative mean expression ± SEM from six independent
381 experiments, as shown in the box (N=6).
382 I) Growth of Mtb in macrophages that were left untreated or treated with HR alone or in combination
383 with U18666A and HRS for 3 days. The CFU numbers are represented as mean $\log_{10}$ values ±
384 SEM from triplicate assays of four independent experiments (N = 4).
385 J) Expression of *INSIG1* gene was quantified by qRT-PCR. *GAPDH* expression values were used
386 as controls for normalization. The relative expression in the *INSIG1* silenced cells was compared
387 with the scrambled control and is represented as Rel. fold change mean ± SEM of triplicate assays
388 from three independent experiments (N=3).
389 K) The levels of mature SREBP2 or β- actin were analyzed by specific immunoblotting of the
390 protein lysates from *INSIG1-silenced* macrophages (Upper panel) and in THP1 macrophages left
391 untreated or treated with 3μg/ml BFA (Lower panel). Levels of β-actin expression were used as
392 the control.
393 L) Growth of Mtb in macrophages left untreated or treated with HR, HRS alone, or in combination
394 with brefeldin A (BFA) for 3 days. The CFU numbers are represented as mean $\log_{10}$ values ± SEM
395 from triplicate assays of three independent experiments (N = 3).
396 P values less than 0.05, 0.01, and 0.005 are represented as *, ** and ***, respectively.
397

398 **Loss of lysosomal integrity couples SRT-mediated cholesterol accumulation with**
399 **activation of inflammasomes.**
400 Accumulation of cholesterol in lysosomes has been associated with a significant damage to the
401 lysosomal membrane, resulting in the formation of pores, a process called lysosomal membrane
402 permeabilization (LMP) [23,25]. This loss of membrane integrity is rapidly repaired by the recruitment
403 of the ESCRT complex via the lectin-galectin 3 [26]. Treatment with SRT significantly induced the
404 expression of *LGALS3* in Mtb infected macrophages (Figure 6A-B). To check if SRT compromised
405 the membrane integrity of lysosomes, cells expressing GFP-tagged galectin 3 were treated with
406 SRT. As observed in Figure 6C, galectin3 was distributed uniformly in the untreated cells, in
407 contrast to the punctate signal in the cells treated with LLOme, a dipeptide documented to induce
408 lysosomal damage [27]. Interestingly, SRT- treated cells also displayed punctate signals, unlike the
409 treatment with citalopram (Figure 6D), suggestive of extensive lysosomal damage. A close
410 connect between the host lysosomal cholesterol levels and mitochondrial function has been
411 established [28-30]. Accumulation of cholesterol in the lysosomes has been associated with altered
412 mitochondrial physiology, exacerbated ROS production, and disorders [31-34]. Given our previous
413 observation for an important role for inflammasome activation by SRT [9] via the induction of
414 mitochondrial ROS [10] and an elegant study by Guo et.al, 2018 establishing a direct link between
415 the activation of SREBP2 and inflammasome induction [35], the role of cholesterol accumulation by
416 SRT as a putative cause of inflammasome activation was evaluated in Mtb infections. In line with
417 our previous studies, while SRT induces significant ROS, citalopram failed to activate
418 mitochondrial ROS in macrophages (Figure 6E-G). A direct link between the host cell cholesterol
419 accumulation, increased SREBP2 activation, and inflammasome activity was probed in cells by
420 estimating the levels of IL1β secretion in the different macrophages. Inhibition of SRT-mediated
421 SREBP2 activation in SCAP-deficient cells reduced the secreted IL1β levels (Figure 6H). This
422 study firmly establishes the importance of the affinity of cationic amphiphilic drugs to the NPC1

protein in augmenting bacterial control, thereby providing a novel target for the future development of host-directed therapy against infections.

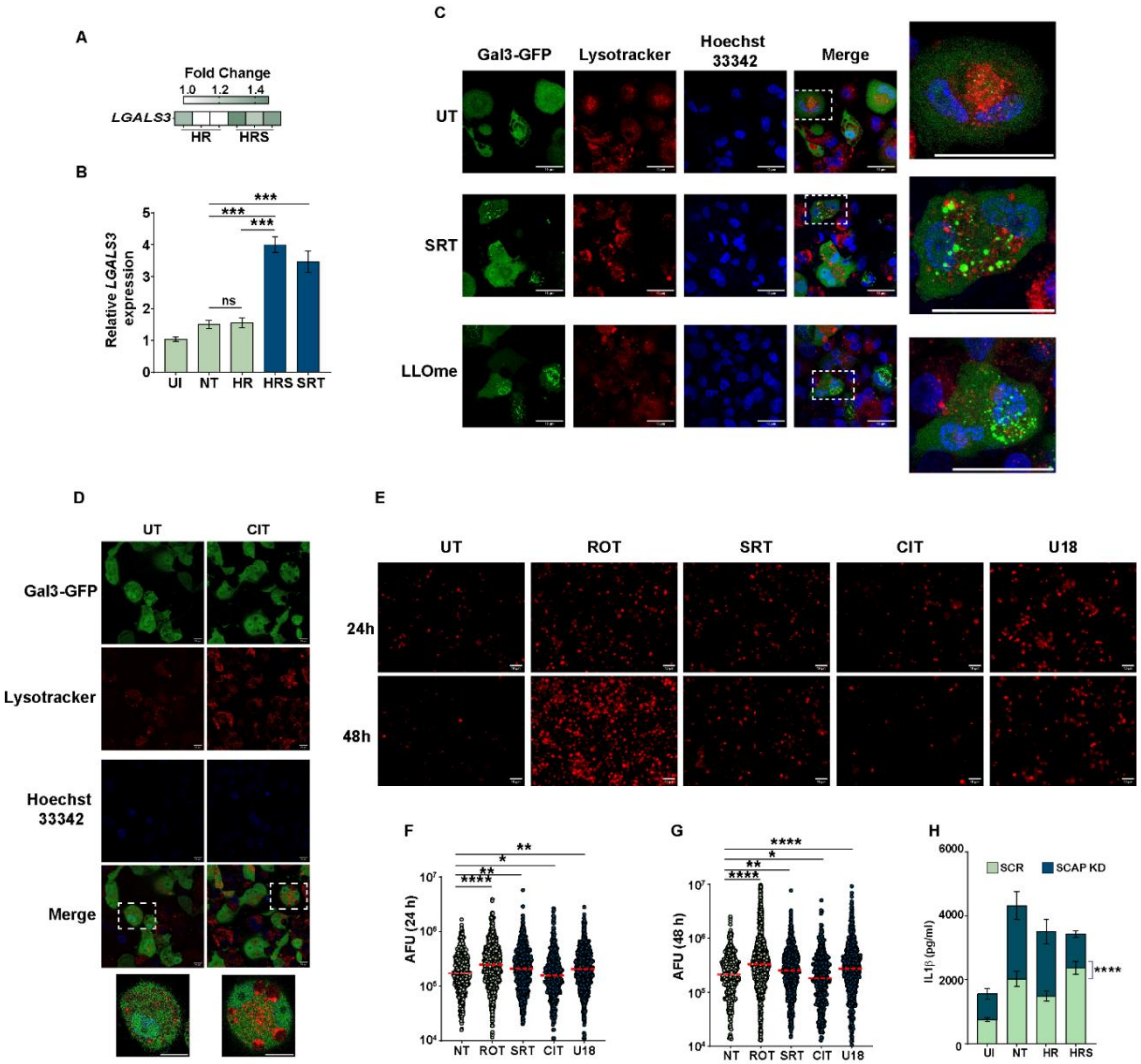

Figure 6

Figure 6: SRT-induced lysosomal cholesterol accumulation induces macrophage inflammasome

(A-B) Gene expression of *LGALS3* (A) in the transcriptomics data and quantified by qRT-PCR (B) in the Mtb-infected macrophages after 18 hours of treatment with HR, HRS, and SRT. The relative

464 expression of specific genes relative to *GAPDH* is represented as fold change ± SEM of triplicate
465 assays of three independent experiments (N=3).
466 (C) Representative images of macrophages overexpressing GFP-tagged galectin 3 protein
467 treated with SRT for 24 hours or LLOme for 15 min and stained with lysotracker Red. Boxes
468 indicate insets, magnified on the right. Scale bar = 10μm.
469 (D) Images after citalopram treatment for 24h in GFP-tagged galectin3 overexpressing
470 macrophages. The inset represents the zoom-in. Scale bar = 10μm.
471 (E-G) Representative images showing mitoSox staining after treatment with sertraline (SRT),
472 citalopram (CIT), U18666A (U18), and rotenone (ROT) as the positive control for mitochondrial
473 ROS induction. The extent of ROS was quantified after 24 h (F) and 48 h (G) of treatment and is
474 represented as arbitrary fluorescence units (AFU) from ~ 800 cells of three independent
475 experiments (N=3).
476 (H) IL-1β levels in the supernatants of Mtb-infected SCR and *SCAP-silenced* cells following
477 treatment with HR or HRS, compared to the untreated group.
478 P values less than 0.05, 0.01 and 0.005 are represented as *, ** and *** respectively.
479
480 **Discussion:**
481 Infection control by innate immune cells is a complex process with the involvement of multiple
482 modalities, intertwining metabolic and inflammatory response pathways to ensure pathogen
483 removal [36,37]. The complexity only increases with the pathogen adept at modifying signaling
484 cascades and occupying intracellular niches that are designed for infection control [38,39]. The
485 incidence of TB, particularly, has been strongly associated with severe malnutrition[38,39].
486 Epidemiological data suggest a strong inverse correlation between serum cholesterol levels and
487 TB incidence and mortality, with TB patients displaying severe hypocholesterolemia [40-42]. In fact,
488 the enhanced levels of sputum sterilization in a small set of pulmonary TB patients on a
489 cholesterol-rich diet only highlight the importance of improving sterol levels for improved treatment

490 outcomes[43]. Recent studies have also implicated a significant role of cholesterol and its
491 derivatives in dictating macrophage response dynamics [44,45]. In line with these observations, we
492 identified an important role for the host cell cholesterol metabolic flux in the antibiotic-mediated
493 potentiation of Mtb control by SRT.
494 In this context, we demonstrate that SRT treatment enhances macrophage cholesterol
495 biosynthesis and import programs through robust activation of the SREBP2 pathway, leading to
496 elevated intracellular cholesterol. We thus reasoned that altering cholesterol flux in macrophages
497 would modulate the effects of sertraline. To our surprise, sertraline activity remained unaltered
498 even in conditions of restricted biosynthesis via statins [46]. Contrary to our expectations, SRT
499 treatment in the presence of statins, increased the expression of the cholesterol biosynthetic
500 genes in macrophages, resulting in enhanced effect of antibiotics in controlling infection, implying
501 the compensatory activation of alternative pathways to maintain homeostasis of cholesterol in
502 cells. Notably, the SREBP2 axis emerged as a critical focal point connecting cholesterol
503 metabolism and infection control in macrophages. In concordance with recent studies that
504 suggest a direct role for statins, we also observed significant activation of SREBP2 with SRT
505 treatment in macrophages, necessary for increased bacterial control [47-49]. However, both genetic
506 perturbation (silencing *SCAP*) and pharmacological activation (BFA), but not silencing of *INSIG1*
507 (induced by SRT in macrophages), confirmed the essential role of this pathway in SRT-mediated
508 Mtb restriction.
509 Our data relates the altered cholesterol trafficking and storage as vital mediators of SRT function.
510 Recently, TMEM97, a cholesterol-responsive NPC1-binding protein, has been implicated in
511 cholesterol trafficking between lysosomes and ER; RNA-interference mediated restraint of
512 TMEM97 reduces lysosomal lipid storage and restores cholesterol levels in the ER in cell models
513 of NPC1 [50]. SRT-treated macrophages with increased expression of TMEM97 (Data not shown)
514 resonate with phenotypes of Niemann-Pick type C disease, with cholesterol-laden lysosomes and
515 disrupted ER-lysosome crosstalk. Along similar lines, treatment with the potent NPC1 inhibitor

516 U18666A induced significant dysregulation of cholesterol trafficking from lysosomes to the
517 endoplasmic reticulum (ER). Consistent with this, cells treated with either SRT or U18666A—but
518 not with citalopram—exhibited markedly enlarged lysosomes, indicative of cholesterol
519 accumulation.

520 This lysosomal sequestration appears to be a key trigger for downstream immune responses.
521 Oxysterols, particularly 25-hydroxy cholesterol (25HC), a dominant negative regulator of
522 cholesterol biosynthesis [51]acts as a dampener of inflammation, preventing the overstimulation of
523 macrophages by downregulating cholesterol biosynthesis and SREBP2 processing, in addition to
524 activating the esterification of excess free cholesterol [52,53]. 25HC is documented to protect
525 macrophages against mitochondria induced NLRP3 inflammasome activation with ch25h$^{-/-}$
526 macrophages the gene encoding for 25HC, elaborating significantly high levels of IL1β in
527 response to LPS stimulation [54,55]. Mitochondrial ROS, SCAP-SREBP2, and the *FASN* effectively
528 mediate NLRP3-mediated inflammasome activation in cells [35,56,57]. Reduced expression of *CH25H*
529 (2-fold) and upregulation of *FASN* (~ 3-fold) suggest a coordinated suppression of anti-
530 inflammatory oxysterol signaling and a shift towards an activated inflammatory state. This
531 metabolic-inflammatory axis distinguishes SRT from related SSRIs such as citalopram, which
532 lacks these effects. In contrast, citalopram had an insignificant effect on these processes, thereby
533 validating the critical role of host cell cholesterol metabolism in macrophage-mediated control of
534 Mtb. These findings further support a model in which host cell cholesterol metabolism plays a
535 critical role in regulating mitochondrial stress and inflammasome activation, thereby contributing
536 to macrophage-mediated control of Mtb.

537 Further, the observed increase in assembly of galectin 3 close to the lysosomes in SRT-treated
538 macrophages advocates for extensive lysosomal membrane permeabilization (LMP) as a result
539 of lysosomal cholesterol accumulation, which is a property of lysosomotrophic molecules like
540 cationic amphiphilic drugs (CADs) [58]. While similar effects were observed with SRT and U18666A,
541 with strong experimental evidence as a CAD, citalopram, a less well-documented cationic

542 amphiphile, failed to bind to NPC-1 protein directly to induce cholesterol accumulation and
543 resultant LMP.
544 Our findings advance a previously understudied axis of reprogramming macrophage cholesterol
545 metabolism and the consequent induction of a lysosomal stress response that enhances
546 inflammasome activation and bacterial clearance (as seen with SRT). These findings emphasize
547 the significance of evaluating host metabolic programs for the design of future adjunct therapies
548 for infection control, specifically in the population cohorts with malnutrition and dyslipidemia.
549 Taken together, our work integrates lipid metabolism and innate immune signaling and places
550 host cholesterol metabolism as a crucial determinant of TB pathogenesis and treatment outcome.

551 **Author contribution**

552 KB and VR were instrumental in the design of the work. KB, RS, NB, JK, MM, and DS were
553 involved in the conduct of the work. SJ and SB were involved in the analysis of the transcriptome
554 high throughput data. None of the authors have any conflict of interest.

555 **Acknowledgements**

556 The authors thank CSIR (VR- MLP2106) for supporting the study. CSIR-STS0016 is
557 acknowledged for continuous maintenance of BSL3 and ABSL2 facilities. CSIR- BSC0403 is duly
558 acknowledge for the microscopy facility. The student fellowships from CSIR- India (KB) are
559 acknowledged. Biorender.com is duly acknowledged for the graphical abstract preparation. The
560 authors thank Ms. Garima Maurya and Mr. Lakshay Kumar for proofreading and suggestions on
561 improving the manuscript. The authors thank Dr. Michael Glickman for the LPDS media.

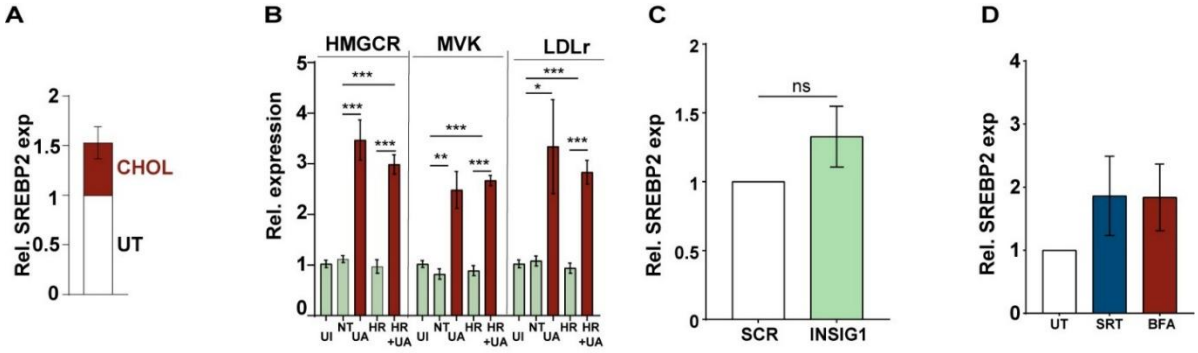

Figure S1

A) The extent of SREBP2 activation was evaluated in macrophages left untreated or treated with cholesterol for 24h by immunoblotting and densitometric analysis of the lysates. Levels of β- actin expression were used as the control. The relative levels of mSREBP2 in cholesterol-treated cells (w.r.t. untreated) are represented as relative mean expression ± SEM from three independent experiments, is shown in the box (N=3).

B) Expression of genes for cholesterol biosynthesis was quantified by qRT-PCR in the Mtb-infected macrophages left untreated or after 18 hours of treatment with HR with and without U8666A (UA). The relative expression of specific genes relative to GAPDH is represented as fold change + SEM of triplicate assays of three independent experiments (N=3).

C, D) The extent of SREBP2 activation was evaluated in SCR or *INSIG1-silenced* macrophages (C) or left untreated or treated with 3μg/ml brefeldin A (D) for 24h by immunoblotting and densitometric analysis of the lysates. Levels of β-actin expression were used as the control. The relative levels of mSREBP2 in cells (w.r.t. untreated) are represented as relative mean expression ± SEM from three independent experiments, as shown in the box (N=3).

589 **Table S1 : Binding interactions predicted for the best docked poses of each ligand**
590

Cholesterol		
Amino acid	**Ligand atom**	**Distance in Å**
Hydrophobic interactions		
PHE86	C19	3.73
L154	C25	3.64
W167	C27	3.68
Y170	C24	3.98
M171	C18	3.35
N176	C21	3.67
Q178	C21	3.51
A179	C12	3.18
F181	C2	3.95
I183	C2	3.33
Hydrogen bonds		
T90	O1	2.80
U18666A		
Amino acid	**Ligand atom**	**Distance in Å**
Hydrophobic interactions		
W5	C13	3.86
Q57	C16	3.16
T60	C16	3.54
L61	C15	3.51
N64	C23	3.88

L65	C23	3.77
F86	C23	3.48
F86	C3	3.34
F86	C7	3.59
T90	C11	3.37
A179	C25	3.99
F181	C14	3.91
I183	C6	3.27
Hydrogen bonds		
N19	O2	1.86
Sertraline		
Amino acid	**Ligand atom**	**Distance in Å**
Hydrophobic interactions		
N64	C8	3.73
L65	C8	3.13
P68	C9	3.26
F86	C7	3.08
Q178	C3	3.74
Hydrogen bonds		
A64	N11	1.99
Citalopram		
Amino acid	**Ligand atom**	**Distance in Å**

Hydrophobic interactions		
L61	C17	3.30
N64	C15	3.85
L65	C13	3.81
F86	C18	3.23
F86	C10	3.56
F86	C15	3.34
A179	C09	3.52
Hydrogen bonds		
T90	N04	2.35
pi-pi stacking		
F86		3.95

591

592 **STAR METHODS**

593 **KEY RESOURCE TABLE**

REAGENT or RESOURCE	SOURCE	IDENTIFIER
Antibodies		
Rabbit polyclonal anti- SREBP2	Invitrogen	Cat# PA1-338
Mouse monoclonal anti-β-actin	Santa Cruz biotechnology	Cat#sc-47778
Bacterial and virus strains		
Mtb Erdman strain	Animal passaged strain EF2	NA

Chemicals, peptides, and recombinant proteins		
HiGlutaXL-RPMI-1640	Himedia	Cat# AL060G
DMEM high glucose	Himedia	Cat# AL007A
Sodium pyruvate	Himedia	Cat# TCL015
Fetal bovine serum	Himedia	Cat# RM9955
Fetal bovine serum lipid depleted	Biowest	Cat# S180L
Phorbol 12-Mysristate 13-acetate(PMA)	SIGMA	Cat# P8139
Ethambutol dihydrochloride	SIGMA	Cat# E4630
Isoniazid	SIGMA	Cat# I3377
Rifampicin	Himedia	Cat# CMS1889
Pyrazinamide carboxamide	SIGMA	Cat# P7136
Sertraline	SIGMA	Cat# S6319
Citalopram hydrobromide	SIGMA	Cat#C7861
U18666A	SIGMA	Cat#U3633
Simvastatin	SIGMA	Cat#S6196
Cholesterol	SIGMA	Cat#C3045
1,10 Phenanthroline	SIGMA	Cat#131377
Brefeldin A	Invitrogen	Cat#00450651
NBD- cholesterol	Avanti	Cat# 810250P
LysoTracker Red DND-99	Invitrogen	Cat#L7528
Hoechst 33342	Gift	NA
Filipin III readymade solution	SIGMA	Cat# SAE0087
Rotenone	SIGMA	Cat# R8875

MitoSox dye	Thermo Fisher Scientific	Cat# M36008
Lipofectamine LTX reagent with Plus reagent	Thermo Fisher Scientific	Cat# 15338100
Puromycin dihydrochloride	Himedia	Cat# TC198
Cholroform EMPARTA grade	Merck	Cat# 1.07024.2500
Methanol HPLC grade	Merck	Cat# 60600725001730
16% methanol free formaldehyde	Thermo Fisher Scientific	Cat# 28908
Critical commercial assays		
BCA protein estimation kit	GBiosciences	Cat#786-571
Total cholesterol	Abcam	Cat#ab282928
Human IL-1β ELISA kit	BD	Cat#557953
ECL Western Blotting Substrate	Promega	Cat#W1015
Deposited data		
RNA sequencing		
Experimental models: Cell lines		
THP1/NT shRNA	This study	N/A

THP1/SCAP shRNA#1	This study	N/A
THP1/SCAP shRNA#2	This study	N/A
THP1/SCAP shRNA#3	This study	N/A
THP1/Insig1 shRNA#1	This study	N/A
THP1/Insig1 shRNA#2	This study	N/A
THP1/Insig1 shRNA#3	This study	N/A
THP1/GFP-tagged Gal3 overexpression	This study	N/A
Oligonucleotides		
Human *GAPDH* primer forward: 5'-GAAGGTGAAGGTCGGAGTC-3'	This study	N/A
Human *GAPDH* primer reverse: 5'-GAAGATGGTGATGGGATTTC-3'	This study	N/A
Human *ACSS2* primer forward: 5'-CATCAGCTTCTGGTCCAAGTG-3'	This study	N/A
Human *ACSS2* primer reverse: 5'-GCTGGAATCCAAGATCCGTTCAC-3'	This study	N/A
Human *HMGCS1* primer forward: 5'-CTCCCTGACGTGGAATGTCT-3'	This study	N/A
Human *HMGCS1* primer reverse: 5'-GAACTGTCTGCCCAGGTGAT-3'	This study	N/A
Human *HMGCR* primer forward: 5'-GACGTGAACCTATGCTGGTCAG-3'	This study	N/A

Human *HMGCR* primer reverse: 5'-GGTATCTGTTTCAGCCACTAAGG-3'	This study	N/A
Human *MVK* primer forward: 5'-CACCTCAGAGCAAGTGGAGAAG-3'	This study	N/A
Human *MVK* primer reverse: 5'-TGCTGCCAGACACACCGAGTAG-3'	This study	N/A
Human *MVD* primer forward: 5'-CTCGGTGAAGTCCTTGCTGATG-3'	This study	N/A
Human *MVD* primer reverse: 5'-AGCGCGATGAAGAGCTGGTTC-3'	This study	N/A
Human *IDI1* primer forward: 5'-CTCCTGGCAGAGATGTGTATCC-3'	This study	N/A
Human *IDI1* primer reverse: 5'-CGGCTGGATTGCTTAATGGATG-3'	This study	N/A
Human *NSDHL* primer forward: 5'-GGATCGGTGGCTCTGGATTC-3'	This study	N/A
Human *NSDHL* primer reverse: 5'-GCAGAGGTCACCCAGAAAG-3'	This study	N/A
Human *SQLE* primer forward: 5'-CTCCAAGTTCAGGAAAAGCCTGC-3'	This study	N/A
Human *SQLE* primer reverse: 5'-GAGAACTGGACTCGGGTTAGCT-3'	This study	N/A
Human *CYP51A1* primer forward: 5'-CTCTTACCAGGTTGGCTGCCTT-3'	This study	N/A
Human *CYP51A1*primer reverse:	This study	N/A

5’-CTTGAGACTGTCTGCGTTTCTGG-3’		
Human *DHCR7* primer forward: 5’-CAGCGCCAGAGACTGCAAA-3’	This study	N/A
Human *DHCR7* primer reverse: 5’-CAGCTTGAATCAAACCACTTCCC-3’	This study	N/A
Human *FDFT1* primer forward: 5’-TGTGACCTCTGAACAGGAGTGG-3’	This study	N/A
Human *FDFT1* primer reverse: 5’-CCCATAGAGTTGGCACGTTCTG-3’	This study	N/A
Human *LDLR* primer forward: 5’-CACGAAGTCAGGAAGATG-3’	This study	N/A
Human *LDLR* primer reverse: 5’-GGGTGCTGCAGATCATTC-3’	This study	N/A
Human *SREBF2* primer forward: 5’-GCTGCCAAGGAGAGTCTATAC-3’	This study	N/A
Human *SREBF2* primer reverse: 5’-GGCCTGAGGTTTCACCAAG-3’	This study	N/A
Human *SCAP* primer forward: 5’-CAAGAACCTCCTGGCAGTAG-3’	This study	N/A
Human *SCAP* primer reverse: 5’-CATGGAAGCGTTCCCAGTC-3’	This study	N/A
Human *INSIG1* primer forward: 5’-TAGCCCTGGTGCTCAAC-3’	This study	N/A
Human *INSIG1* primer reverse: 5’-AGCACTGGCGTGGTTAATG-3’	This study	N/A

Human *LGALS3* primer forward: 5'-GATGCGTTATCTGGGTCTGG-3'	This study	N/A
Human *LGALS3* primer reverse: 5'-GCACTTGGCTGTCCAGAAGATG-3'	This study	N/A
Human *ABCA1* primer forward: 5'-GATGCGTTATCTGGGTCTGG-3'	This study	N/A
Human *ABCA1* primer reverse: 5'-GCACTTGGCTGTCCAGAAGATG-3'	This study	N/A
Human *ACAT1* primer forward: 5'-CAGTAACAGCTGCCAATGC-3'	This study	N/A
Human *ACAT1* primer reverse: 5'-GGTTCTACAGCAGCGTCAG-3'	This study	N/A
Recombinant DNA		
SCAP shRNA#1	Horizon (Dharmacon)	Cat#V3SH11240_227412984
SCAP shRNA#2	Horizon (Dharmacon)	Cat#V3SH11240_228955440
SCAP shRNA#3	Horizon (Dharmacon)	Cat#V3SH11240_228534848
Insig1 shRNA#1	Horizon (Dharmacon)	Cat#V3SH11240_227321339
Insig1 shRNA#2	Horizon (Dharmacon)	Cat#V3SH11240_228332166
Insig1 shRNA#3	Horizon (Dharmacon)	Cat#V3SH11240_226630552

Non-targeting shRNA	Horizon (Dharmacon)	Cat#VSC11716
pcDNA-EF-Gal3_GFP	This study	
Software and algorithms		
ImageJ		https://imagej.net/ij/
GSEA		https://www.gsea-msigdb.org/gsea/index.jsp
Graphpad Prism	PRISM 10	licensed

594

595 **EXPERIMENTAL MODEL DETAILS**

596 **CELL CULTURE**

597 THP1 and THP1 dual monocytes purchased from ECACC were used in this study. Both THP1
598 and THP1 dual monocytes were cultured in RPMI 1640 containing 10% FBS and 1 mM sodium
599 pyruvate at 37^0C in a 5% CO_2 humidified incubator. They were differentiated into macrophages
600 using 100 nM Phorbol-13-myristate 13-acetate (PMA) for 24 hours, followed by media change.
601 Following a resting period of 48 hours, cells were utilized for respective experiments.

602 **BACTERIAL STRAINS AND MEDIA**

603 Mtb Erdmann strain was grown in Middlebrook 7H9 medium with 4% Albumin-dextrose-saline Or
604 Middlebrook 7H10 plates supplemented with 10% oleic acid-albumin-dextrose-catalase (OADC)
605 at 37^0C. A final concentration of 0.05% Tween 80 was added to the liquid medium.

606 **METHOD DETAILS**

607 **RNA sequencing and analysis:**

608 Total RNA was isolated from the Mtb-infected macrophages after treatment with anti-TB drugs
609 (Isoniazid and rifampicin) in the presence or absence of sertraline for 18 hours. Total RNA was

610 used for stranded library preparation and paired-end clustering with 150bp x 2 end of sequencing
611 performed on HiSeqX (Illumina) by Medgenome Labs. Quality check of raw sequenced reads was
612 performed using Fastqc 0.12.1 and summarized with Multiqc 0.4. Adapters (Illumina universal
613 adapters) and poor-quality bases were trimmed using Trimmomatic 0.39. The trimmed reads were
614 aligned to the human genome gtf (v44) using Star (2.7.10b). Finally, the rawcounts matrix was
615 generated using Subread 2.0.6. Differential gene expression analysis was conducted via
616 edgeR3.42.4. Gene set enrichment analysis was used to compare datasets.

617 **Quantitative PCR:**

618 RNA was isolated using RNAzol (Sigma), and cDNA was synthesized using oligo-dT primers
619 using Verso cDNA synthesis kit following the manufacturer's protocol. Quantitative PCR was
620 performed using KAPA SYBR green (Sigma) on a LightCycler480 (Roche).

621 **Total cholesterol estimation:**

622 THP1 monocytes were seeded in a 24-well plate at a density of 0.5*10^6 cells. Cells after washing
623 with 1X PBS were lysed in 100ul of 1% Triton X-100 for 20 mins on ice. Protein was estimated by
624 the BCA protein estimation kit following the protocol given. For total lipid isolation, 400µL of
625 chloroform: methanol (1:2) was added along with 100µL of 50 mM citric acid. The mix was
626 vortexed and spun down. After the addition of 100µL of autoclaved water, the mix was vortexed
627 and spun down, and finally, 100µL of chloroform was added. After centrifugation of the mix at
628 12000g for 10 minutes, the lower phase was collected and vacuum centrifuged for 30 minutes.
629 The pellet was diluted in cholesterol assay buffer, and total cholesterol levels were assessed
630 using the Total Cholesterol & Cholesteryl Ester Colorimetric Assay Kit (ab282928) following the
631 recommended protocol. Values were normalized with the protein content.

632 **Macrophage infection:**

633 The Mtb culture was centrifuged and washed with PBST (1x PBS with 0.05% of Tween 80) twice,
634 and a single cell suspension was made after spinning down the culture at 800g for 10 minutes.

635 THP1 dual macrophages were infected for 6 hours at MOI5. After 6 hours, cells were washed
636 twice with 1X PBS, and appropriate cell culture media was added.

637 **Intracellular bacterial growth assay:**

638 THP1 dual monocytes were seeded in a 48-well plate at a density of 0.15 million cells. Cells were
639 differentiated into macrophages as indicated, and after a 48-hour resting period, cells were
640 infected with Mtb for 6 hours at MOI5. After stopping the infection, cells were treated with drugs
641 isoniazid (20ng/mL), rifampicin (100ng/mL), and sertraline (20μM) given in 10% FBS RPMI media.
642 At day 3 post-treatment, cells were lysed with water containing 0.05% Tween 80, and dilutions of
643 intracellular bacteria were made in PBST. The final diluted lysate was plated on 7H10 plates.
644 To restrict cholesterol uptake by the macrophages, treatment with TB drugs was given in RPMI
645 media supplemented with 10% Lipoprotein-deficient serum (LPDS).
646 For the cholesterol replenishment assay, Mtb-infected THP1 macrophages were treated with
647 cholesterol (2μg/ml) for an hour after infection, followed by incubation with anti-TB drugs in LPDS
648 medium, and further cholesterol was added every 24 hours.

649 **Immunoblotting**

650 THP1 dual macrophages were lysed in RIPA buffer along with a protease inhibitor cocktail.
651 Protein concentration was estimated by BCA assay, and 50μg of total protein was loaded per
652 sample in a 10% polyacrylamide gel. Protein was transferred to a nitrocellulose membrane, and
653 the membrane was blocked using a 5% BSA solution. The membrane was next incubated
654 overnight in anti-rabbit SREBP2 antibody, on shaking at 4°C. Next, the membrane was washed
655 thrice with PBST (1X PBS with 0.05% Tween 20) solution and incubated with HRP-conjugated
656 secondary antibody for an hour at room temperature. After washing with PBST, the membrane
657 was imaged using ImageQuant LAS 500.

658 **Filipin Staining:**

659 The THP1 macrophages were seeded in confocal chamber slides (1.5*10^4 cells per chamber)
660 and treated with sertraline at 20μM for 24 hours. Cells were washed twice with 1x PBS before

661 fixation with 4% methanol-free formaldehyde in 1X PHEM buffer for 20 mins at room temperature.
662 After an additional wash with 1x PBS, cells were stained with filipin staining solution (50ug/ml
663 diluted in 1x PBS) for an hour in the dark at room temperature. Next, the cells were washed with
664 1x PBS and imaged on a Leica SP8 laser scanning confocal microscope. Filipin was excited at
665 the 405nm laser.

666 **Cholesterol compartmentalization assay:**

667 THP1 monocytes were seeded at a density of 0.15 million cells in a four-chamber confocal dish
668 and differentiated as mentioned. The NBD-cholesterol at a final conc of 10μM was added for 24
669 hours along with the different compounds such as sertraline (20μM), citalopram (20μM), and
670 U18666A (2μg/ml). Before initiation of imaging, cells were stained with Lysotracker Red (100nM)
671 along with Hoechst dye for 1 hour in 10% FBS containing RPMI. Images were taken using a Leica
672 SP8 laser scanning confocal microscope.

673 **Stable knockdown/overexpression cell line generation:**

674 Lenti-X 293T cells were transfected with pVSVG and pDR2.8 plasmids together with lentiviral
675 constructs expressing gene-specific shRNA or non-targeting controls to generate viral particles.
676 After 6 hours of transfection, the media was changed to 2% FBS containing DMEM, and after 48
677 hours, the cell supernatant was collected and centrifuged at 100g for 5 minutes to remove cell
678 debris. Further, this supernatant was filtered through a 0.45μ syringe filter, and viral particles were
679 concentrated using a 30kDa centricon filter. For transduction in THP1 monocytes, 50,000 cells
680 were seeded in a 24-well plate, and 100μL of viral stock was added along with a final
681 concentration of 8μg/mL polybrene. After 24 hours media was changed, and antibiotic selection
682 was initiated after 48 hours of transduction with 0.6μg/mL of puromycin. Cells showing tRFP
683 fluorescence co-expressed with shRNA were checked regularly.

684 The hGal3 and eGFP are excised from the pEGFP-hGal3 plasmid using Nhe1, Nde1, and Msc1
685 restriction enzymes and ligated to Xba1 and Msc1 digested pcDNA 3.1 vector. The final plasmid
686 is transfected into THP1 monocytes using Lipofectamine LTX.

687 **Computational assessment of NPC1- SSRI interactions:**

688 A composite structure of NPC- 1 protein (cryo-EM, PDB IDL 6W5V) with the addition of missing
689 atoms (PDB Fixer) [59] and validated for structure quality by Procheck [60] for Ramachandran
690 parameters were used as a template for the analysis of interaction with SSRIs- Sertraline and
691 citalopram. Ligand structures of Cholesterol, U18666A, sertraline, and citalopram from the PDB
692 ligand library were converted from SDF to PDB format using OpenBabel [61]and used for docking
693 studies focused on the binding region reported earlier [23]. The residues reported to interact with
694 sertraline were selected as the binding site region, with the centroid of the binding site used as
695 the center of the grid box with dimensions (40,40,40 npts) for docking analysis with 50 iterations
696 for each ligand by Autodock4.2 [62]. The docked poses were clustered at the default value of 2.0Å
697 RMSD, and the clusters were ranked based on the lowest binding energy in each cluster. The
698 binding energy is calculated in AutoDock as a semi-empirical function of intermolecular forces
699 such as Vanderwaals forces, hydrogen bonds, desolvation energy, electrostatic energy, and
700 torsional energies [63]. The binding energy of the best docked pose, the mean binding energy of
701 the top cluster, and the total number of clusters were noted. The docked pose with the lowest
702 binding energy was visualised using PyMOL, and the protein-ligand interactions were predicted
703 using PLIP [64].

704 **Galectin 3 puncta assessment:**

705 GFP tagged galectin-3 overexpressing THP1 monocytes were seeded in a chambered confocal
706 dish and treated with sertraline (20μM), citalopram (20μM), U18666A (2μg/ml) for 24 hours, and
707 with 1mM LLOMe for 15 minutes. Before imaging, cells were stained with Lyostracker Red and
708 Hoechst for an hour. Images were taken using a Leica SP8 laser scanning confocal microscope.

709 **Mitochondrial ROS estimation:**

710 THP1 dual cells were differentiated as indicated. Treatment was given with rotenone at 10μM for
711 30 minutes or with different indicated compounds. The cells were incubated with 5μM of MitoSox

712 dye for 30 minutes. After washing with 1X PBS, cells were imaged in the Invitrogen™ EVOS™
713 M5000 Imaging System.

714 **ELISA:**

715 THP1 dual macrophages were infected with Mtb at MOI5 and treated with different compounds.
716 Supernatant was collected at the indicated time points and filtered through a 0.2μ filter.
717 Concentration of IL-1β was determined using an ELISA kit following the recommended protocol.

718 **Statistical analysis**

719 The results are depicted as mean ± SEM. Statistical analysis was carried out using Student's t-
720 test (Welch's test or Mann-Whitney test) using GraphPad Prism. P values less than 0.05, 0.01,
721 0.005 are represented as *, ** and *** respectively.

722

723 **References:**

724 1. Chakaya, J., Petersen, E., Nantanda, R., Mungai, B.N., Migliori, G.B., Amanullah, F.,
725 Lungu, P., Ntoumi, F., Kumarasamy, N., Maeurer, M., and Zumla, A. (2022). The WHO
726 Global Tuberculosis 2021 Report - not so good news and turning the tide back to End
727 TB. Int J Infect Dis *124 Suppl 1*, S26-S29. 10.1016/j.ijid.2022.03.011.
728 2. Global tuberculosis report 2024. (2024).
729 3. Trajman, A., Campbell, J.R., Kunor, T., Ruslami, R., Amanullah, F., Behr, M.A., and
730 Menzies, D. (2025). Tuberculosis. Lancet *405*, 850-866. 10.1016/S0140-6736(24)02479-
731 6.
732 4. Tobin, E.H., and Tristram, D. (2025). Tuberculosis Overview. In StatPearls.
733 5. Matteelli, A., Lovatti, S., Rossi, B., and Rossi, L. (2025). Update on multidrug-resistant
734 tuberculosis preventive therapy toward the global tuberculosis elimination. Int J Infect
735 Dis *155*, 107849. 10.1016/j.ijid.2025.107849.
736 6. Nahid, P., Mase, S.R., Migliori, G.B., Sotgiu, G., Bothamley, G.H., Brozek, J.L.,
737 Cattamanchi, A., Cegielski, J.P., Chen, L., Daley, C.L., et al. (2019). Treatment of Drug-
738 Resistant Tuberculosis. An Official ATS/CDC/ERS/IDSA Clinical Practice Guideline. Am
739 J Respir Crit Care Med *200*, e93-e142. 10.1164/rccm.201909-1874ST.
740 7. Young, C., Walzl, G., and Du Plessis, N. (2020). Therapeutic host-directed strategies to
741 improve outcome in tuberculosis. Mucosal Immunol *13*, 190-204. 10.1038/s41385-019-
742 0226-5.
743 8. Wong, E.B., Cohen, K.A., and Bishai, W.R. (2013). Rising to the challenge: new
744 therapies for tuberculosis. Trends Microbiol *21*, 493-501. 10.1016/j.tim.2013.05.002.
745 9. Shankaran, D., Singh, A., Dawa, S., Arumugam, P., Gandotra, S., and Rao, V. (2023).
746 The antidepressant sertraline provides a novel host directed therapy module for
747 augmenting TB therapy. Elife *12*. 10.7554/eLife.64834.
748 10. Singh, A., Bisht, K., Yadav, N., Nanda, R., and Rao, V. (2025). Inflammasome activation
749 dictates the efficacy of antimycobacterial activity of frontline TB drugs. bioRxiv,
750 2025.2004.2002.646750. 10.1101/2025.04.02.646750.

751 11. King, R.J., Singh, P.K., and Mehla, K. (2022). The cholesterol pathway: impact on
752 immunity and cancer. Trends Immunol *43*, 78-92. 10.1016/j.it.2021.11.007.
753 12. Canfran-Duque, A., Rotllan, N., Zhang, X., Andres-Blasco, I., Thompson, B.M., Sun, J.,
754 Price, N.L., Fernandez-Fuertes, M., Fowler, J.W., Gomez-Coronado, D., et al. (2023).
755 Macrophage-Derived 25-Hydroxycholesterol Promotes Vascular Inflammation,
756 Atherogenesis, and Lesion Remodeling. Circulation *147*, 388-408.
757 10.1161/CIRCULATIONAHA.122.059062.
758 13. Reboldi, A., and Dang, E. (2018). Cholesterol metabolism in innate and adaptive
759 response. F1000Res *7*. 10.12688/f1000research.15500.1.
760 14. de Freitas, F.A., Levy, D., Reichert, C.O., Cunha-Neto, E., Kalil, J., and Bydlowski, S.P.
761 (2022). Effects of Oxysterols on Immune Cells and Related Diseases. Cells *11*.
762 10.3390/cells11081251.
763 15. Cyster, J.G., Dang, E.V., Reboldi, A., and Yi, T. (2014). 25-Hydroxycholesterols in innate
764 and adaptive immunity. Nat Rev Immunol *14*, 731-743. 10.1038/nri3755.
765 16. Duewell, P., Kono, H., Rayner, K.J., Sirois, C.M., Vladimer, G., Bauernfeind, F.G., Abela,
766 G.S., Franchi, L., Nunez, G., Schnurr, M., et al. (2010). NLRP3 inflammasomes are
767 required for atherogenesis and activated by cholesterol crystals. Nature *464*, 1357-1361.
768 10.1038/nature08938.
769 17. Schonewille, M., de Boer, J.F., Mele, L., Wolters, H., Bloks, V.W., Wolters, J.C.,
770 Kuivenhoven, J.A., Tietge, U.J., Brufau, G., and Groen, A.K. (2016). Statins increase
771 hepatic cholesterol synthesis and stimulate fecal cholesterol elimination in mice. J Lipid
772 Res *57*, 1455-1464. 10.1194/jlr.M067488.
773 18. Chen, L., Zhang, J., Xu, W., Chen, J., Tang, Y., Xiong, S., Li, Y., Zhang, H., Li, M., and
774 Liu, Z. (2024). Cholesterol-rich lysosomes induced by respiratory syncytial virus promote
775 viral replication by blocking autophagy flux. Nat Commun *15*, 6311. 10.1038/s41467-
776 024-50711-4.
777 19. Eid, W., Dauner, K., Courtney, K.C., Gagnon, A., Parks, R.J., Sorisky, A., and Zha, X.
778 (2017). mTORC1 activates SREBP-2 by suppressing cholesterol trafficking to lysosomes
779 in mammalian cells. Proc Natl Acad Sci U S A *114*, 7999-8004.
780 10.1073/pnas.1705304114.
781 20. Radhakrishnan, A., Ikeda, Y., Kwon, H.J., Brown, M.S., and Goldstein, J.L. (2007).
782 Sterol-regulated transport of SREBPs from endoplasmic reticulum to Golgi: oxysterols
783 block transport by binding to Insig. Proc Natl Acad Sci U S A *104*, 6511-6518.
784 10.1073/pnas.0700899104.
785 21. Frolov, A., Zielinski, S.E., Crowley, J.R., Dudley-Rucker, N., Schaffer, J.E., and Ory,
786 D.S. (2003). NPC1 and NPC2 regulate cellular cholesterol homeostasis through
787 generation of low density lipoprotein cholesterol-derived oxysterols. J Biol Chem *278*,
788 25517-25525. 10.1074/jbc.M302588200.
789 22. Peake, K.B., and Vance, J.E. (2010). Defective cholesterol trafficking in Niemann-Pick
790 C-deficient cells. FEBS Lett *584*, 2731-2739. 10.1016/j.febslet.2010.04.047.
791 23. Alvarez-Valadez, K., Sauvat, A., Diharce, J., Leduc, M., Stoll, G., Guittat, L.,
792 Lambertucci, F., Paillet, J., Motino, O., Ferret, L., et al. (2025). Lysosomal damage due
793 to cholesterol accumulation triggers immunogenic cell death. Autophagy *21*, 934-956.
794 10.1080/15548627.2024.2440842.
795 24. DeBose-Boyd, R.A., Brown, M.S., Li, W.P., Nohturfft, A., Goldstein, J.L., and
796 Espenshade, P.J. (1999). Transport-dependent proteolysis of SREBP: relocation of site-
797 1 protease from Golgi to ER obviates the need for SREBP transport to Golgi. Cell *99*,
798 703-712. 10.1016/s0092-8674(00)81668-2.
799 25. Hu, P., Li, H., Sun, W., Wang, H., Yu, X., Qing, Y., Wang, Z., Zhu, M., Xu, J., Guo, Q.,
800 and Hui, H. (2021). Cholesterol-associated lysosomal disorder triggers cell death of

801 hematological malignancy: Dynamic analysis on cytotoxic effects of LW-218. Acta
802 Pharm Sin B *11*, 3178-3192. 10.1016/j.apsb.2021.02.004.
803 26. Aits, S., Kricker, J., Liu, B., Ellegaard, A.M., Hamalisto, S., Tvingsholm, S., Corcelle-
804 Termeau, E., Hogh, S., Farkas, T., Holm Jonassen, A., et al. (2015). Sensitive detection
805 of lysosomal membrane permeabilization by lysosomal galectin puncta assay.
806 Autophagy *11*, 1408-1424. 10.1080/15548627.2015.1063871.
807 27. Thiele, D.L., and Lipsky, P.E. (1990). The action of leucyl-leucine methyl ester on
808 cytotoxic lymphocytes requires uptake by a novel dipeptide-specific facilitated transport
809 system and dipeptidyl peptidase I-mediated conversion to membranolytic products. J
810 Exp Med *172*, 183-194. 10.1084/jem.172.1.183.
811 28. Davis, O.B., Shin, H.R., Lim, C.Y., Wu, E.Y., Kukurugya, M., Maher, C.F., Perera, R.M.,
812 Ordonez, M.P., and Zoncu, R. (2021). NPC1-mTORC1 Signaling Couples Cholesterol
813 Sensing to Organelle Homeostasis and Is a Targetable Pathway in Niemann-Pick Type
814 C. Dev Cell *56*, 260-276 e267. 10.1016/j.devcel.2020.11.016.
815 29. Martin, L.A., Kennedy, B.E., and Karten, B. (2016). Mitochondrial cholesterol:
816 mechanisms of import and effects on mitochondrial function. J Bioenerg Biomembr *48*,
817 137-151. 10.1007/s10863-014-9592-6.
818 30. de la Mata, M., Cotan, D., Villanueva-Paz, M., de Lavera, I., Alvarez-Cordoba, M.,
819 Luzon-Hidalgo, R., Suarez-Rivero, J.M., Tiscornia, G., and Oropesa-Avila, M. (2016).
820 Mitochondrial Dysfunction in Lysosomal Storage Disorders. Diseases *4*.
821 10.3390/diseases4040031.
822 31. Goicoechea, L., Conde de la Rosa, L., Torres, S., Garcia-Ruiz, C., and Fernandez-
823 Checa, J.C. (2023). Mitochondrial cholesterol: Metabolism and impact on redox biology
824 and disease. Redox Biol *61*, 102643. 10.1016/j.redox.2023.102643.
825 32. Balboa, E., Castro, J., Pinochet, M.J., Cancino, G.I., Matias, N., Saez, P.J., Martinez, A.,
826 Alvarez, A.R., Garcia-Ruiz, C., Fernandez-Checa, J.C., and Zanlungo, S. (2017). MLN64
827 induces mitochondrial dysfunction associated with increased mitochondrial cholesterol
828 content. Redox Biol *12*, 274-284. 10.1016/j.redox.2017.02.024.
829 33. Lin, J.X., Xu, C.Y., Wu, X.M., Che, L., Li, T.Y., Mo, S.M., Guo, D.B., Lin, Z.N., and Lin,
830 Y.C. (2023). Rab7a-mTORC1 signaling-mediated cholesterol trafficking from the
831 lysosome to mitochondria ameliorates hepatic lipotoxicity induced by aflatoxin B1
832 exposure. Chemosphere *320*, 138071. 10.1016/j.chemosphere.2023.138071.
833 34. Mari, M., Morales, A., Colell, A., Garcia-Ruiz, C., and Fernandez-Checa, J.C. (2009).
834 Mitochondrial glutathione, a key survival antioxidant. Antioxid Redox Signal *11*, 2685-
835 2700. 10.1089/ARS.2009.2695.
836 35. Guo, C., Chi, Z., Jiang, D., Xu, T., Yu, W., Wang, Z., Chen, S., Zhang, L., Liu, Q., Guo,
837 X., et al. (2018). Cholesterol Homeostatic Regulator SCAP-SREBP2 Integrates NLRP3
838 Inflammasome Activation and Cholesterol Biosynthetic Signaling in Macrophages.
839 Immunity *49*, 842-856 e847. 10.1016/j.immuni.2018.08.021.
840 36. Hu, T., Liu, C.H., Lei, M., Zeng, Q., Li, L., Tang, H., and Zhang, N. (2024). Metabolic
841 regulation of the immune system in health and diseases: mechanisms and interventions.
842 Signal Transduct Target Ther *9*, 268. 10.1038/s41392-024-01954-6.
843 37. Andersson, M., Aronsen, K.F., Balch, C., Domellof, L., Eksborg, S., Hafstrom, L.O.,
844 Howell, S.B., Karesen, R., Midander, J., and Teder, H. (1989). Pharmacokinetics of
845 intra-arterial mitomycin C with or without degradable starch microspheres (DSM) in the
846 treatment of non-resectable liver cancer. Acta Oncol *28*, 219-222.
847 10.3109/02841868909111250.
848 38. Omotade, T.O., and Roy, C.R. (2019). Manipulation of Host Cell Organelles by
849 Intracellular Pathogens. Microbiol Spectr *7*. 10.1128/microbiolspec.BAI-0022-2019.

850 39. Clemente, T.M., Angara, R.K., and Gilk, S.D. (2023). Establishing the intracellular niche
851 of obligate intracellular vacuolar pathogens. Front Cell Infect Microbiol *13*, 1206037.
852 10.3389/fcimb.2023.1206037.
853 40. Perez-Guzman, C., and Vargas, M.H. (2006). Hypocholesterolemia: a major risk factor
854 for developing pulmonary tuberculosis? Med Hypotheses *66*, 1227-1230.
855 10.1016/j.mehy.2005.12.041.
856 41. Jo, Y.S., Han, K., Kim, D., Yoo, J.E., Kim, Y., Yang, B., Choi, H., Sohn, J.W., Shin, D.W.,
857 and Lee, H. (2021). Relationship between total cholesterol level and tuberculosis risk in
858 a nationwide longitudinal cohort. Sci Rep *11*, 16254. 10.1038/s41598-021-95704-1.
859 42. Chidambaram, V., Zhou, L., Ruelas Castillo, J., Kumar, A., Ayeh, S.K., Gupte, A., Wang,
860 J.Y., and Karakousis, P.C. (2021). Higher Serum Cholesterol Levels Are Associated
861 With Reduced Systemic Inflammation and Mortality During Tuberculosis Treatment
862 Independent of Body Mass Index. Front Cardiovasc Med *8*, 696517.
863 10.3389/fcvm.2021.696517.
864 43. Parivakkam Mani, A., K, S., K, D.K., and Yadav, S. (2023). Assessment of Lipid Profile
865 in Patients With Pulmonary Tuberculosis: An Observational Study. Cureus *15*, e39244.
866 10.7759/cureus.39244.
867 44. Bah, S.Y., Dickinson, P., Forster, T., Kampmann, B., and Ghazal, P. (2017). Immune
868 oxysterols: Role in mycobacterial infection and inflammation. J Steroid Biochem Mol Biol
869 *169*, 152-163. 10.1016/j.jsbmb.2016.04.015.
870 45. Hayakawa, S., Tamura, A., Nikiforov, N., Koike, H., Kudo, F., Cheng, Y., Miyazaki, T.,
871 Kubekina, M., Kirichenko, T.V., Orekhov, A.N., et al. (2022). Activated cholesterol
872 metabolism is integral for innate macrophage responses by amplifying Myd88 signaling.
873 JCI Insight *7*. 10.1172/jci.insight.138539.
874 46. Istvan, E.S., and Deisenhofer, J. (2001). Structural mechanism for statin inhibition of
875 HMG-CoA reductase. Science *292*, 1160-1164. 10.1126/science.1059344.
876 47. Xu, J.F., Washko, G.R., Nakahira, K., Hatabu, H., Patel, A.S., Fernandez, I.E., Nishino,
877 M., Okajima, Y., Yamashiro, T., Ross, J.C., et al. (2012). Statins and pulmonary fibrosis:
878 the potential role of NLRP3 inflammasome activation. Am J Respir Crit Care Med *185*,
879 547-556. 10.1164/rccm.201108-1574OC.
880 48. Henriksbo, B.D., Lau, T.C., Cavallari, J.F., Denou, E., Chi, W., Lally, J.S., Crane, J.D.,
881 Duggan, B.M., Foley, K.P., Fullerton, M.D., et al. (2014). Fluvastatin causes NLRP3
882 inflammasome-mediated adipose insulin resistance. Diabetes *63*, 3742-3747.
883 10.2337/db13-1398.
884 49. Altaf, A., Qu, P., Zhao, Y., Wang, H., Lou, D., and Niu, N. (2015). NLRP3 inflammasome
885 in peripheral blood monocytes of acute coronary syndrome patients and its relationship
886 with statins. Coron Artery Dis *26*, 409-421. 10.1097/MCA.0000000000000255.
887 50. Ebrahimi-Fakhari, D., Wahlster, L., Bartz, F., Werenbeck-Ueding, J., Praggastis, M.,
888 Zhang, J., Joggerst-Thomalla, B., Theiss, S., Grimm, D., Ory, D.S., and Runz, H. (2016).
889 Reduction of TMEM97 increases NPC1 protein levels and restores cholesterol trafficking
890 in Niemann-pick type C1 disease cells. Hum Mol Genet *25*, 3588-3599.
891 10.1093/hmg/ddw204.
892 51. Nishimura, T., Inoue, T., Shibata, N., Sekine, A., Takabe, W., Noguchi, N., and Arai, H.
893 (2005). Inhibition of cholesterol biosynthesis by 25-hydroxycholesterol is independent of
894 OSBP. Genes Cells *10*, 793-801. 10.1111/j.1365-2443.2005.00879.x.
895 52. Choi, H., Kim, H.J., Lee, S.E., Song, H.H., Kim, J., Han, J., Jeong, J.H., Lee, D.Y.,
896 Chang, S., and Mook-Jung, I. (2025). 25-Hydroxycholesterol modulates microglial
897 function and exacerbates Alzheimer's disease pathology: mechanistic insights and
898 therapeutic potential of cholesterol esterification inhibition. J Neuroinflammation *22*, 50.
899 10.1186/s12974-025-03357-y.

53. Griffiths, W.J., and Wang, Y. (2022). Cholesterol metabolism: from lipidomics to immunology. J Lipid Res *63*, 100165. 10.1016/j.jlr.2021.100165.
54. Reboldi, A., Dang, E.V., McDonald, J.G., Liang, G., Russell, D.W., and Cyster, J.G. (2014). Inflammation. 25-Hydroxycholesterol suppresses interleukin-1-driven inflammation downstream of type I interferon. Science *345*, 679-684. 10.1126/science.1254790.
55. Viaud, M., Ivanov, S., Vujic, N., Duta-Mare, M., Aira, L.E., Barouillet, T., Garcia, E., Orange, F., Dugail, I., Hainault, I., et al. (2018). Lysosomal Cholesterol Hydrolysis Couples Efferocytosis to Anti-Inflammatory Oxysterol Production. Circ Res *122*, 1369-1384. 10.1161/CIRCRESAHA.117.312333.
56. Zhou, R., Yazdi, A.S., Menu, P., and Tschopp, J. (2011). A role for mitochondria in NLRP3 inflammasome activation. Nature *469*, 221-225. 10.1038/nature09663.
57. Leishman, S., Aljadeed, N.M., Qian, L., Cockcroft, S., Behmoaras, J., and Anand, P.K. (2024). Fatty acid synthesis promotes inflammasome activation through NLRP3 palmitoylation. Cell Rep *43*, 114516. 10.1016/j.celrep.2024.114516.
58. Kuzu, O.F., Toprak, M., Noory, M.A., and Robertson, G.P. (2017). Effect of lysosomotropic molecules on cellular homeostasis. Pharmacol Res *117*, 177-184. 10.1016/j.phrs.2016.12.021.
59. Eastman, P., Swails, J., Chodera, J.D., McGibbon, R.T., Zhao, Y., Beauchamp, K.A., Wang, L.P., Simmonett, A.C., Harrigan, M.P., Stern, C.D., et al. (2017). OpenMM 7: Rapid development of high performance algorithms for molecular dynamics. PLoS Comput Biol *13*, e1005659. 10.1371/journal.pcbi.1005659.
60. Laskowski, R.A., Rullmannn, J.A., MacArthur, M.W., Kaptein, R., and Thornton, J.M. (1996). AQUA and PROCHECK-NMR: programs for checking the quality of protein structures solved by NMR. J Biomol NMR *8*, 477-486. 10.1007/BF00228148.
61. O'Boyle, N.M., Banck, M., James, C.A., Morley, C., Vandermeersch, T., and Hutchison, G.R. (2011). Open Babel: An open chemical toolbox. J Cheminform *3*, 33. 10.1186/1758-2946-3-33.
62. Morris, G.M., Huey, R., Lindstrom, W., Sanner, M.F., Belew, R.K., Goodsell, D.S., and Olson, A.J. (2009). AutoDock4 and AutoDockTools4: Automated docking with selective receptor flexibility. J Comput Chem *30*, 2785-2791. 10.1002/jcc.21256.
63. Huey, R., Morris, G.M., Olson, A.J., and Goodsell, D.S. (2007). A semiempirical free energy force field with charge-based desolvation. J Comput Chem *28*, 1145-1152. 10.1002/jcc.20634.
64. Salentin, S., Schreiber, S., Haupt, V.J., Adasme, M.F., and Schroeder, M. (2015). PLIP: fully automated protein-ligand interaction profiler. Nucleic Acids Res *43*, W443-447. 10.1093/nar/gkv315.